The structure and photoluminescence performances of $Zn_xAl_2O_4:Cr^{3+}$ crystals with various annealing temperatures

A. P. ZHOU[a*], D. ZHANG[b,*], Z. Q. GONG[c], Q. SHI[b], C. LI[a]
[a] *School of Physics and Optoelectronic Engineering , Shandong University of Technology , Zibo 255049, China*
[b] *School of Physical Science and Information Technology, Liaocheng University, Liaocheng 252059, China*
[c] *School of Materials Science and Engineering, Shandong University of Science and Technology, Qingdao 266590, China*

$Zn_xAl_2O_4$: Cr^{3+} (0.1 mol%) crystals were synthesized by using sol-gel method follow by the annealing treatment with temperatures ranging from 600 °C to 1000 °C. A series of emission peaks associated with the spin-forbidden $^2E_g \rightarrow {}^4A_{2g}$ transition of Cr^{3+} ions were observed at the range from 650 nm to 720 nm. With the Zn/Al molar ratio increasing, the results of X-ray photoelectron spectra showed that the excess Al ions occupying tetrahedral sites decreased. Meanwhile the full width at half maximum of emission peaks became much narrower, and the intensity ratio between R line and N line increased for all samples but decreased with the annealing temperature increasing.

(Received May 30, 2017; accepted October 10, 2018)

Keywords: Semiconductors, $ZnAl_2O_4$ crystals, Spinel structure, Photoluminescence

1. Introduction

As a wide bandgap semiconductor (~3.8 eV) [1-3], zinc aluminate ($ZnAl_2O_4$) has attracted much attention due to its thermal stability, chemical stability, and potential applications in the field of catalysis [4,5] and display (cathodoluminescence) [6,7]. In order to achieve effective luminescence, the rare earth elements were most considered as dopant ions in spinel structure, such as Eu^{2+}, Dy^{3+} and Tb^{3+} for $SrAl_2O_4$, $CaAl_2O_4$, $ZnAl_2O_4$, and so on [8-10]. However, the scarcity of rare earth elements hinders the large-scale practical applications. Recently, some researchers found that the band gap of $ZnAl_2O_4$ can be tuned effectively by transition metals doping so as to obtain luminescences with desired wavelengths. Zhang et al. [11] investigated the photoluminescence of $ZnAl_2O_4$ crystals doped with Mn^{2+} ions, which exhibits an excellent green emission at about 512 nm owning to the Mn^{2+} ions located in tetrahedral sites within the spinel structure, and a red emission related to the Mn^{3+} and Mn^{4+} ions located in octahedral sites within the spinel structure. Besides green and red emissions, blue emissions associated with localized levels in the band gap were presented for Co doped zinc aluminates [12]. Afterwards, a strong and broad blue emission from $ZnAl_2O_4$:Ti crystals was reported by Tsai et al. [13]. So, the researches on the transition metals doping in semiconductors as substitutes for rare earth elements are urgently needed.

$ZnAl_2O_4$ has a normal spinel crystal structure with Fd3m space group, in which the tetrahedrally coordinated Zn sites (T_d) are surrounded by four oxygen ions and octahedrally coordinated Al sites (O_h) are surrounded by six oxygen ions. The 32 oxygen ions are C_{3v} sites arranged in a close-packed cubic formation leaving 64 tetrahedral (T_d) and 32 distorted (D_{3d}) sites. The Mn ions with different valences should occupy different sites in spinel structure, which resulted in emissions with different wavelengths. The Cr^{3+} ions occupying the octahedral sites result in the red emissions at 687 nm and 689 nm [14,15]. While some defects related to the antisite, such as Zn^{2+} ions occupying the sites of Al^{3+} ions and Al^{3+} ions occupying the sites of Zn^{2+} ions, which cause the energy level further splitting and new emissions ranging from 698 nm to 713 nm.

This work presents the structural and photoluminescence properties of $ZnAl_2O_4:Cr^{3+}$ nanocrystals with various Zn/Al molar ratio under various annealing temperature prepared by using the sol-gel method, in which a series of red visible emissions originating from the efficient energy transition of $^4A_{2g} \rightarrow {}^4T_{1g}(F)$ and $^4A_{2g}(F) \rightarrow {}^4T_{2g}(F)$ of Cr^{3+} are clearly observed under 410 nm and 530 nm excitation, respectively. And the intensity ratio between R line and N line reveals obvious increase with Zn/Al molar ratio.

2. Experimental details

The starting materials were $Zn(NO_3)_2 \cdot 6H_2O$, $Al(NO_3)_3 \cdot 9H_2O$, $CrCl_3 \cdot 6H_2O$ and ethylene glycol (Shanghai Aladdin Bio-Chem Technology Co., LTD). The theoretical composition of $Zn_xAl_2O_4:Cr_{0.001}$ (x=0.8, 1.0, 1.2, respectively) powders were prepared by using sol-gel method. Mixtures containing $Zn(NO_3)_2 \cdot 6H_2O$, $Al(NO_3)_3 \cdot 9H_2O$ and $CrCl_3 \cdot 6H_2O$ were first dissolved in deionized water. The mixed solution was stirred for 30 min, and ethylene glycol was introduced into the slurry as stabilizer. The transparent sols were kept at 200 °C in an oven until gelation. At last, the puffed products were calcined for 3 h to obtain $Zn_xAl_2O_4:Cr^{3+}$ nanophosphors at 600 °C, 800 °C and 1000 °C, respectively.

The microstructure of $Zn_xAl_2O_4:Cr^{3+}$ phosphors was investigated by using X-ray diffractometer (XRD) with Cu-Ka radiation ($\lambda = 0.15406$ nm). Fourier transform infrared spectra in the range of 400-2000 cm^{-1} were recorded by using a Bruker IFS66 v/s spectrometer. The morphologies were characterized by using scanning electron microscope (SEM, FEI Sirion, Holland) and transmission electron microscope (TEM, JEOL-2000). The X-ray photoelectron spectroscopy (XPS) analysis was carried out with a Thermol scientific Escalab 250Xi using monochromatized Al Kα X-ray source. The PL spectra were measured with Spectro-fluorophotometer (FLS920, Edinburgh) and 450 W Xe-lamp was used as the excitation source.

3. Results and discussion

3.1. Structural properties

Fig. 1 shows the x-ray diffraction (XRD) patterns of $Zn_xAl_2O_4:Cr^{3+}$ crystals with various annealing temperatures. The typical diffraction peaks corresponding to the spinel structure of zinc aluminate (JCDPS: 82-1043) are observed for all the samples. For the samples with $x = 1.2$, the impurities related to ZnO are presented. With the increasing of annealing temperature and the value of x, the intensity of all the XRD diffraction peaks increases, while the full width at half maximum (FWHM) decreases, which indicate that the crystallite size becomes larger. According to the Scherrer's equation [16], the mean grain sizes along (311) orientation are calculated, as shown in Fig. 2. As the annealing temperature increases from 600 °C to 1000 °C, the grain size reveals a weak increase for $Zn_{0.8}Al_2O_4:Cr^{3+}$ crystals. In spite of the smaller crystalline size for x=1.2 compared to the case of x=0.8 at the annealing temperature of 600 °C, a sharp increase occurs when the annealing temperature is elevated to 1000 °C. It indicates that the crystals with spinel structure can be formed easily in rich-zinc atmosphere.

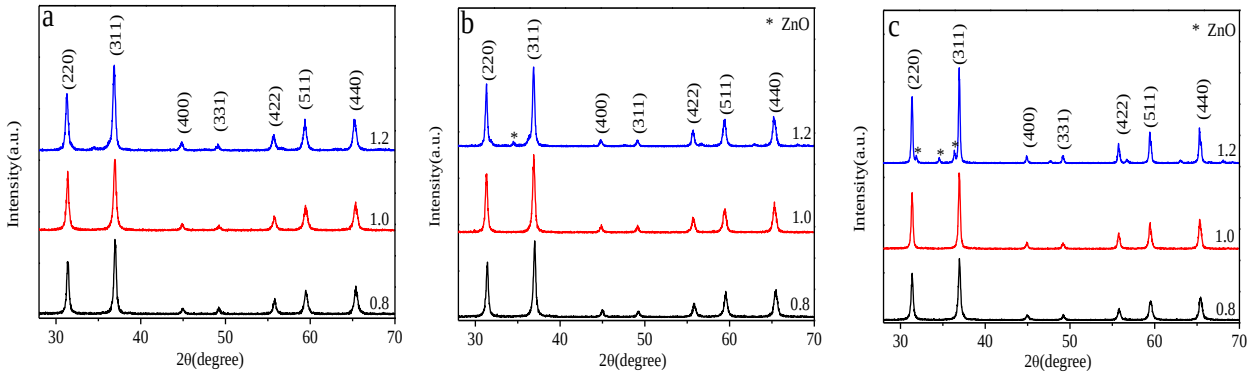

Fig. 1. XRD patterns of $Zn_xAl_2O_4:Cr^{3+}$ crystals with various annealing temperatures. (a) 600 °C; (b) 800 °C; (c) 1000 °C

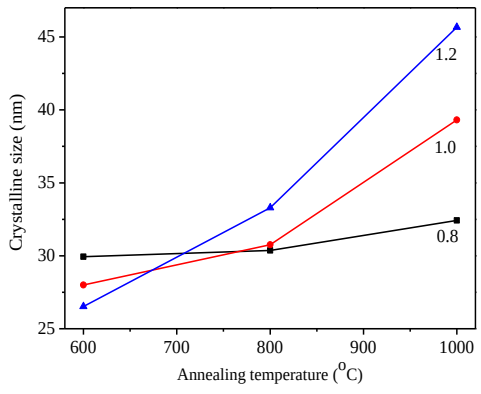

Fig. 2. The mean crystallite size of $Zn_xAl_2O_4:Cr^{3+}$ crystals

Fig. 3 gives the angular dependence of $Zn_xAl_2O_4:Cr^{3+}$ crystals on the annealing temperatures and x values. The diffraction peak shift, which implies different defects existing in crystal lattices. According to the results of nuclear magnetic resonance (NMR) from Sreeja et al. [17], the defects related to Al at tetrahedral sites and oxygen vacancies exist on the surface of crystals with standard stoichiometry in precursors. For the powders synthesized at rich-Al atmosphere, some defects related to the zinc vacancies should be presented in the lattices. With concentration increasing of zinc source in precursors, more and more Zn^{2+} ions enter the spinel lattices, which causes the diffraction peaks shift toward lower diffraction angle because of the larger

radius of Zn^{2+} than that of Al^{3+} (0.74 Å VS. 0.5 Å).

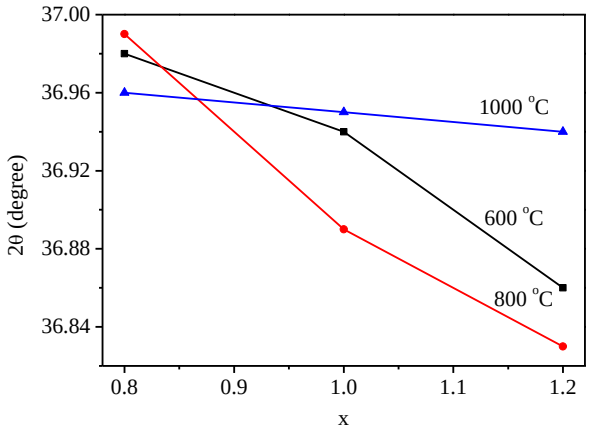

Fig. 3. The diffraction angles of (311) peaks with respect to x for $Zn_xAl_2O_4:Cr^{3+}$ crystals

Fig. 4 illustrates the FT-IR spectrum of $Zn_xAl_2O_4:Cr^{3+}$ crystals synthesized at 1000 °C. The functional groups existing in the samples can be deduced from the specific frequencies of the absorption peaks. For all of the investigated samples, peaks at about 3401, 1641, 656, 552 and 493 cm^{-1} are presented. The absorption peaks at 3401 and 1641 cm^{-1} are assigned to the -OH group bending vibration of absorbed water. The peaks at 493, 552 and 656 cm^{-1}, typical spinel structure of zinc aluminate , are assigned to bending vibration of $[AlO_6]$ groups, bending vibration of tetrahedral $[ZnO_4]$ groups and stretching vibration of octahedral $[AlO_6]$ groups, respectively [12, 16, 18-20].

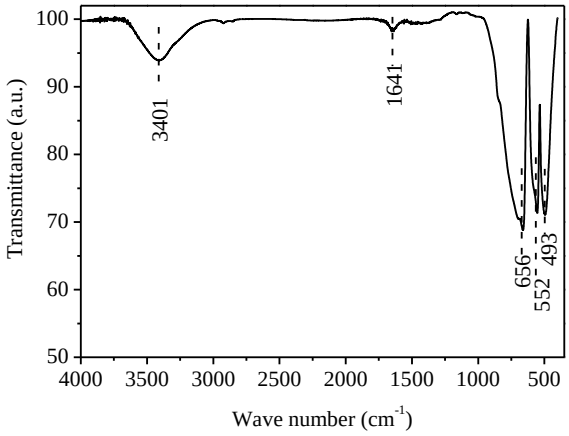

Fig. 4. FT-IR spectrum of $ZnAl_2O_4:Cr^{3+}$ crystals Annealed at 1000 °C

3.2. Morphologies

Fig. 5 shows the SEM images of $Zn_xAl_2O_4:Cr^{3+}$ crystals with annealing temperature at 600 °C and 1000 °C, respectively. It is obvious that the crystallite size reveals an obvious increase with the increase of annealing temperature and Zn/Al molar ratio. It indicates that the crystallinity of $Zn_xAl_2O_4:Cr^{3+}$ can be improved in the rich-Zn atmosphere, which corresponds to the results of XRD.

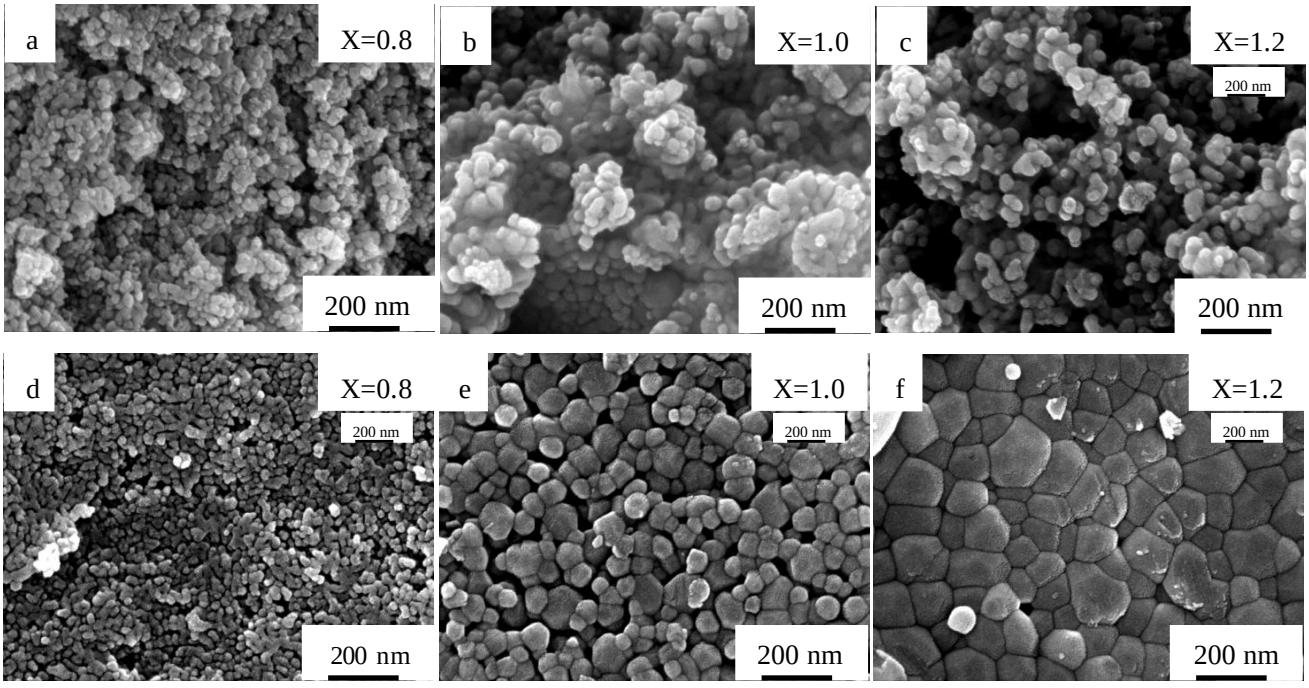

Fig. 5. SEM images of $Zn_xAl_2O_4:Cr^{3+}$ crystals with annealing temperature at (a)-(c) 600 °C and (d)-(f) 1000 °C

In order to investigate the morphology of $Zn_xAl_2O_4:Cr^{3+}$ crystals, the measurement of TEM was carried out, and the corresponding results are shown in Fig. 6. The crystallite size of the samples with x=0.8 is very tiny and agglomerated. With a further increase in Zn/Al molar ratio, the particles reveal an obvious increase in the crystallite size, and become more dispersive. The crystals with x=1.0 reveal uniform crystal sizes, and the larger crystals with x=1.2 become non uniform, as shown in the SEM results.

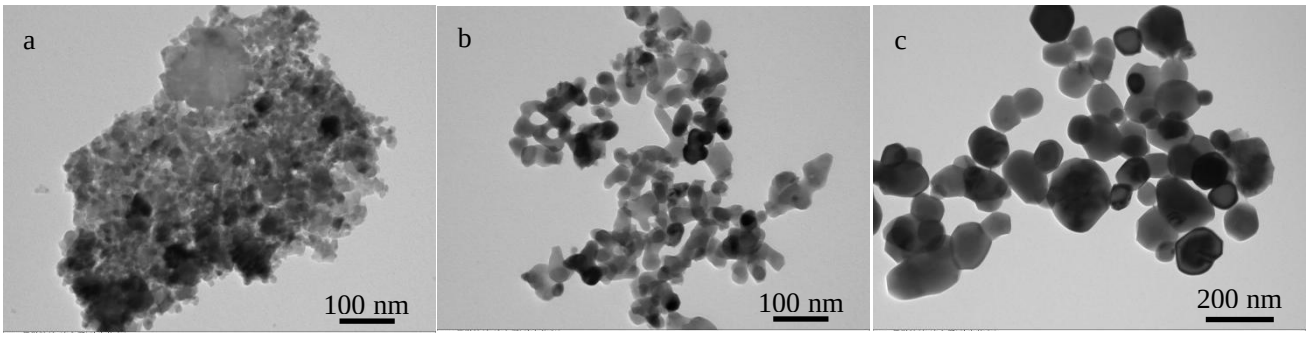

Fig. 6. TEM images of $Zn_xAl_2O_4:Cr^{3+}$ crystals annealed at 1000 °C. (a) x=0.8; (b) x=1.0; (c) x=1.2

3.3. XPS

The XPS spectra of Al 2p in $ZnxAl_2O_4:Cr^{3+}$ crystals are shown in Fig. 7. For all the samples, the experimental data can be fitted well with two Gaussian peaks. The peak at about 73.6 eV is related to Al in [AlO_6] group, and that at about 72.9 eV is related to Al in [AlO_4] group [21,22]. It is obvious that the intensity of peak at 73.6 eV increases and that of peak at 72.9 eV decreases with Zn concentration increasing in precursors. It suggests that excess Al ions should tend to occupy the tetrahedral sites, and with Zn concentration increasing, more and more Zn ions enter the spinel lattices and occupy the tetrahedral sites. However, Al ions in tetrahedral site are still observed in the sample with excess Zn ions (x=1.2).

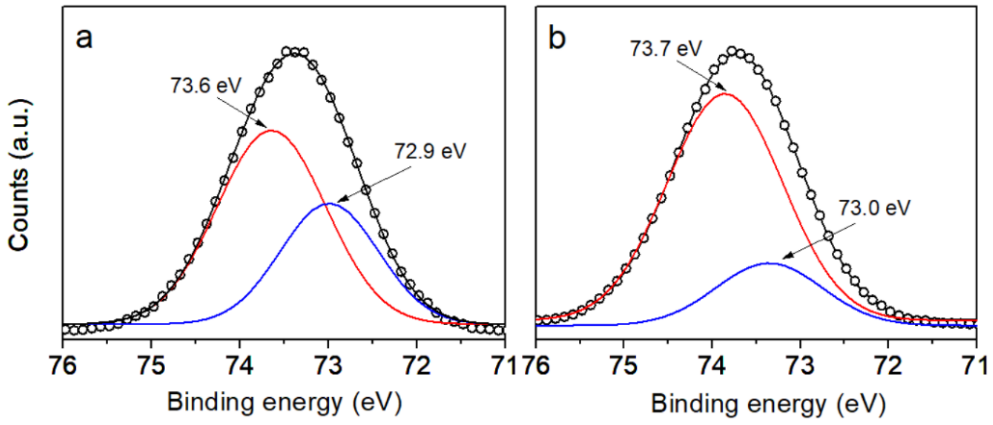

Fig. 7. XPS spectra of Al 2p for $Zn_xAl_2O_4:Cr^{3+}$ crystals. (a) x=0.8; (b) x=1.2

Fig. 8 shows the XPS spectra of Zn 2p in $Zn_xAl_2O_4:Cr^{3+}$ crystals. Two signal peaks are observed for all samples and the experimental data can be fitted well with single Gaussian peak. The peaks at about 1022 eV and 1045 eV can be respectively identified as the Zn2p1/2 and Zn2p3/2 lines in tetrahedral sites ([ZnO4 group]) [23]. Due to the higher formation energy, Zn ions occupying Al sites are not observed in the powders with excess Zn ions. It indicates that the excess Zn ions in precursors cannot absolutely eliminate the antisite defects related to Al occupying Zn sites, but reduce these defects in spinel lattices and improve the crystallinity of zinc aluminate crystals.

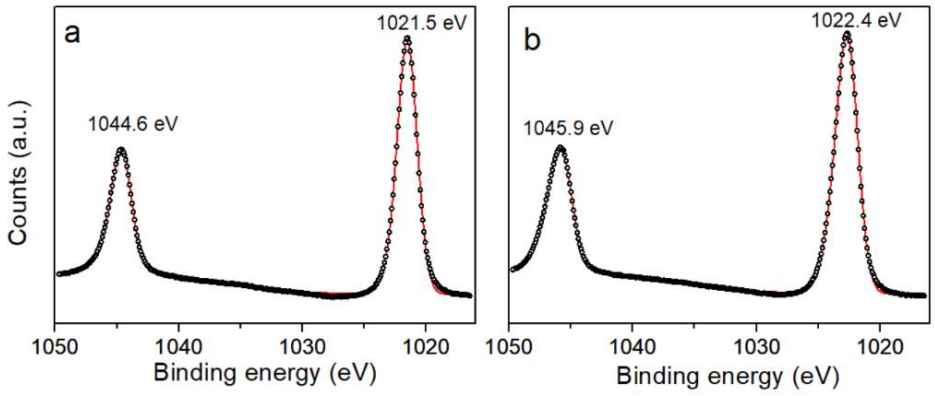

Fig. 8. XPS spectra of Zn 2p for $Zn_xAl_2O_4:Cr^{3+}$ crystals. (a) x=0.8; (b) x=1.2

3.4. PL properties

The typical excitation and emission spectra of $ZnAl_2O_4:Cr^{3+}$ crystals are shown in Fig. 9. When monitoring the emission at 687 nm, the specimen exhibit two main peaks of excitation at 410 nm and 530 nm, suggesting that Cr^{3+} ions are in octahedral symmetry in $ZnAl_2O_4$ lattices. The broad band of 397-421 nm are assigned at $^4A_{2g}(F)\rightarrow{}^4T_{1g}(F)$[24], and the peak located at 530 nm is assigned at $^4A_{2g}(F)\rightarrow{}^4T_{2g}(F)$[14,25]. A series of emission peaks are presented in the PL spectra as shown in Fig. 9. With different excitation wavelengths, the emission peaks show the similar profile but different intensity. For $ZnAl_2O_4$ crystal with spinel structure, the tetrahedral positions are occupied by Zn^{2+} ions (8a positions) and the octahedral positions are occupied by Al^{3+} ions (16d positions). While in the process of crystal growth, some defects in connection with inverse spinel structure forms, resulting in some Al^{3+} ions occupy 8a positions and some Zn^{2+} ions occupy 16d positions [20]. According to the results of Singh et al. [25], the prominent line at 687nm and the adjacent line at 689 nm can be attributed to the regular 16d site of the spinel structure (R lines). The emission peaks at 698 nm, 709 nm and 717 nm reflect the Cr^{3+} ions perturbed by inversion between Zn^{2+} and Al^{3+} within the first two coordination spheres (N lines) [25, 26-28].

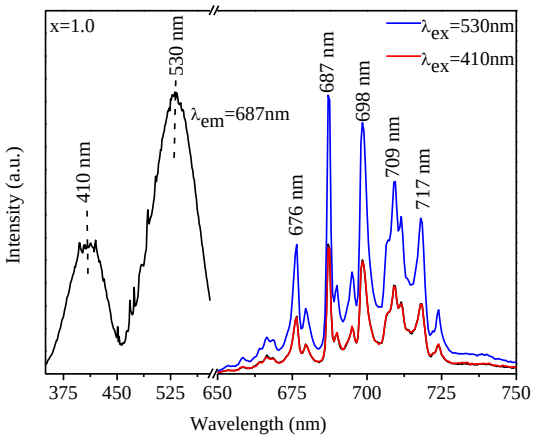

Fig. 9. The excitation and emission spectra of $ZnAl_2O_4:Cr^{3+}$ crystals calcined at 1000 °C

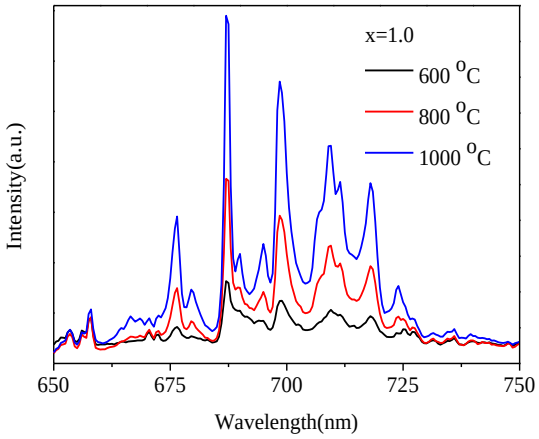

Fig. 10. PL spectra of $ZnAl_2O_4:Cr^{3+}$ crystals with annealing temperature ranging from 600 °C to 1000 °C

With the annealing temperature increasing from 600 °C to 1000 °C, the PL intensity is enhanced as shown in Fig. 10(x=1.0), which is associated with the improvement of crystallinity of $ZnAl_2O_4:Cr^{3+}$ crystals and the better dispersibility of Cr^{3+} ions in spinel lattices of $ZnAl_2O_4$. With the value of x increasing from 0.8 to 1.2, the PL intensity reveals an obvious increase and more narrow full width at half maximum (Fig. 11), indicating that the crystallinity of zinc aluminate should be enhanced in the rich-zinc atmosphere. Considering the sites of Cr^{3+} and Al^{3+} (M^{3+}) in spinel structure, more zinc ions entering spinel lattices can cause some M^{3+} in tetrahedral sites to be transferred into octahedral sites. As a result, the intensity of PL peaks corresponding to R lines should be more intense than that corresponding to N lines. For the investigated samples, the intensity ratios between the PL peaks at 687 nm (R line) and 698 nm (N line) are shown in Fig. 11(d). With the Zn/Al molar ratio increasing, the intensity ratio between R line and N line increases, reflecting that the antisite defects related to Al occupying the sites of Zn are reduced in rich-Zn atmosphere. While the higher annealing temperature supply the conditional

energy for Zn ions to occupy the Al sites in spinel lattices, which makes the intensity ratio between R line and N line decrease. Furthermore, the samples with higher Zn/Al molar ratio reveal the narrower FWHM of emission peaks. The various crystal fields induced by worse crystallinity, resulting in the transition energy shift, then the larger range of emission wavelengths can be observed in emission spectra. When the crystallinity is improved, the band edge becomes sharper, which induces the more narrow emission peaks.

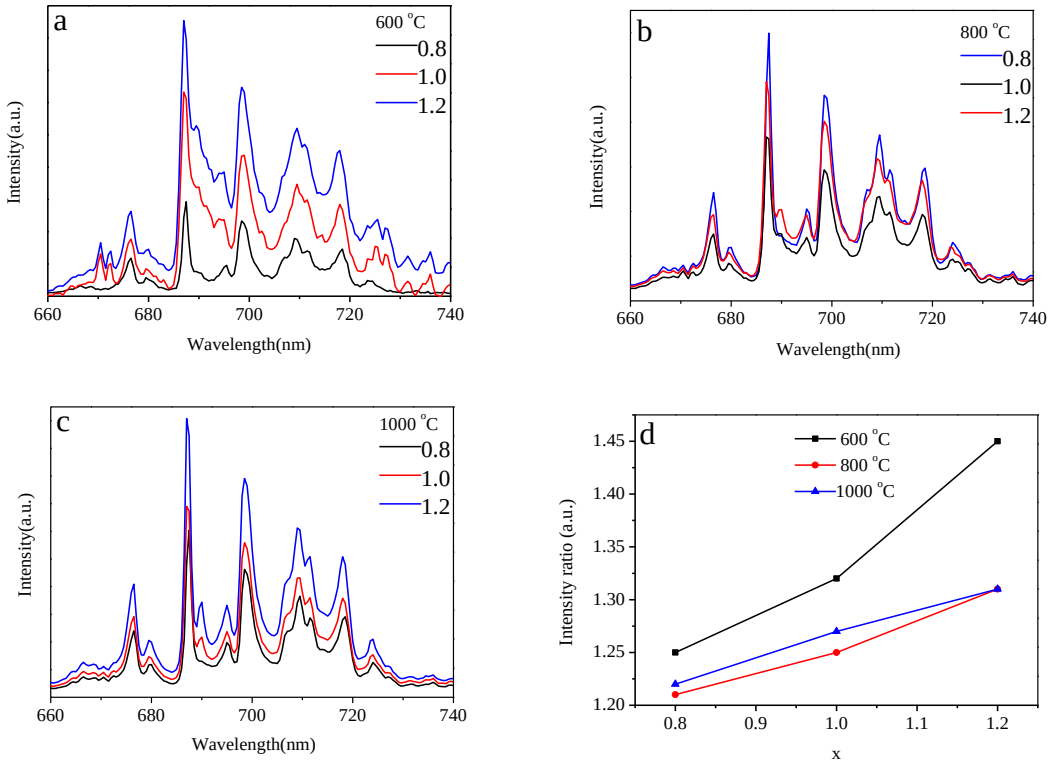

Fig. 11. (a)-(c) PL spectra of $ZnAl_2O_4:Cr^{3+}$ crystals with various Zn^{2+} concentrations and annealing temperatures. (d) The intensity ratio between peaks at 687 nm and 698 nm

4. Conclusions

$Zn_xAl_2O_4:Cr^{3+}$ crystals with spinel structure were synthesized by using sol-gel method and then annealed at various temperatures. The crystallite size is enhanced and the crystallinity is improved with annealing temperature increasing from 600 °C to 1000 °C. Meanwhile, the structure and photoluminescence benefit from the excessive Zn in precursors. More and more Zn ions enter the spinel lattices, especially occupy the tetrahedral sites, which enhances the crystallite size and improves the crystallinity of zinc aluminate crystals. On account of the improving crystallinity, the intensity of emissions related to $^2E_g \rightarrow {}^4A_{2g}$ transition of Cr^{3+} ions is enhanced and the FWHM decreases to about 1 nm. The presence of N lines in PL spectra of all samples suggests that it is inevitable for the Al^{3+} ions to occupy the tetrahedral sites. Although the intensity of N lines increases with the Zn/Al molar ratio increasing, the intensity ratio between R line and N line reveals an obvious increase, indicating that the antisite defects are reduced for the samples with excessive zinc source in precursors. With increasing annealing temperature, the inversion defects reveal an increase due to the higher additional energy supplied by annealing process.

Acknowledgement

This work was supported by Natural Science Foundation of Shandong Province(No. ZR2014JL032), Natural Science Foundation of Shandong Province(No. ZR2016EMM01), Initial Foundation for Doctor Programme of Liaocheng University (No. 318051410), and the Project of Science and Technology Plan for University of Shandong Province (No. J16LJ05).

References

[1] S. V. Montloung, F. B. Dejene, H. C. Swart, O. M. Ntwaeaborawa, Ceram. Int. **41**(5), 6776 (2015).
[2] S. V. Motloung, F. B. Dejene, L. F. Koao, et al., Opt. Mater. **64**, 26 (2017).
[3] S. G Menon, D. N. Hebbar, S. D. Kulkarni, et al., Mater. Res. Bull. **86**, 63 (2017).
[4] X. F. Zhao, L. Wang, X. Xu, et al., AIChE J. **58**(2),

573 (2012).
[5] S. G Menon, K. S. Choudhari, S. A. Shivashankar, et al., J. Alloy. Compd. **728**, 484 (2017).
[6] E. Martinez-Sanchez, M. Garcia-Hipolito, J. Guzman, et al., Status. Solidi. A **202**(1), 102 (2005).
[7] T. Nagura, H. Kominami, Y. Nakanishi, K. Hara, J. Magn. Reson. **48**(9), 400 (2009).
[8] T. Matsuzawa, Y. Aoki, N. Takeuchi, et al., J. Electrochem. Soc. **143**(8), L243 (1996).
[9] T. Kinoshita, M. Yamazaki, H. Kawazoe, H. Hosono, J. Appl. Phys. **86**(7), 3729 (1999).
[10] X. Y. Chen, C. Ma, Opt. Mater. **32**(3), 415 (2010).
[11] D. Zhang, C. Z. Wang, Y. L. Liu, et al., J. Lumin. **132**(6), 1529 (2012).
[12] G T. Anand, L. J. Kennedy, J. J. Vijaya, J. Alloy Compd. **581**, 558 (2013).
[13] M. T. Tsai, Y. S. Chang, Y. H. Chou, K. M. Tsai, J. Solid State Chem. **214**(28), 86 (2014).
[14] D. Zhang, X. X. Ma, Q. Zhang, et al., J. Alloy. Compd. **688**, 581(2016).
[15] D. Zhang, Y. H. Qiu, Y. R. Xie, et al., Mater. Design. **115**, 37 (2017).
[16] D. L. Ge, Y. J. Fan, C. L. Qi, Z. X. Sun, J. Mater. Chem. A **1** (5), 1651 (2013).
[17] V. Sreeja, T. S. Smitha, D. Nand, et al., J. Phys. Chem. C **112**, 14737 (2008).
[18] R. E. Rojas-Hernandez, F. R. Ubio-Marcos, M. Á. Rodriguez, et al., Mater. Design. **108**, 354 (2016).
[19] A. A. D. Silva, A. De Souza Goncalves, M. R. Davolos, J. Sol-Gel Sci. Technol. **49**(1), 101 (2009).
[20] I. B. Huang, Y. S. Chang, H. L. Chen, et al., Thin Solid Films **570**, 451 (2014).
[21] K. G Tshabalala, S. H. Cho, J. K. Park, et al., J. Alloys. Comp. **509**, 10115 (2011).
[22] S. Iaiche, A. Djelloul, J. Spectrosc. **19**, 9 (2015).
[23] N. Benito, D. Diaz, L. Vergara, et al., Surf. Coat. Tech. **206**, 1484 (2014).
[24] D. N. Hebbar, S. G Menon, K. S. Choudhari, et al., Journal of the American Ceramic Society **101**(2), 800 (2018).
[25] V. Singh, R. P. S. Chakradhar, J. L. Rao, et al., J. Mater. Sci. **46**(7), 2331 (2001).
[26] G G P. van Gorkom, J. C. M. Henning, R. P. Van Stapele, Phys. Rev. B. **8**(3), 955 (1973).
[27] H. M. Kahan, R. M. Macfarlane, J. Chem, Phys. **54**(12), 5197 (1971).
[28] W. Nie, F. M. Michel-Calendini, C. Linares, et al., J. Lumin. **46**(3), 177 (1990).

*Corresponding author: japzhou@163.com